Compensation of Crosstalk in Three-Axial Induction Magnetometers

Eugene Paperno, Asaf Grosz, Shai Amrusi, and Boris Zadov

***Abstract*—A method for the compensation of crosstalk in three-axial induction magnetometers is developed theoretically and verified experimentally. The compensation is based on deriving crosstalk-free magnetometer outputs from a system of equations describing the magnetometer total outputs as a function of the applied field, the parameters of the magnetometer coils, and the crosstalk factors for the applied and secondary magnetic fluxes. Processing the total outputs of an experimental magnetometer has demonstrated an effective reduction of the crosstalk: it has been reduced below 0.5% in the whole magnetometer bandwidth, including the frequencies near resonance, where the crosstalk is especially strong (20%). In comparison, the reduction of the crosstalk by applying magnetic feedback is much less effective: the crosstalk has been reduced down to 6% at resonance, remained unchanged at low and high frequencies, and even increased just below resonance. Moreover, magnetic feedback flattens the frequency response and significantly reduces the magnetometer selectivity, which can be advantageous in many applications. Employing magnetic feedback also increases the magnetometer complexity and its power consumption.**

***Index Terms*—Compensation, crosstalk, magnetic feedback, three-axial induction magnetometers.**

I. Introduction

INTEGRATION OF search coils [1]–[4] into a three-axial induction magnetometer [5]–[10] (see Fig. 1) causes inevitable crosstalk [9], [10] between them. The crosstalk degrades the magnetometer orthogonality and, hence, the accuracy of measuring the magnitude and direction of an applied field.

The crosstalk occurs by two mechanisms [9]: the first is related to the distribution of the applied flux [see Fig. 2(a)], and the second is related to the distribution of the secondary fluxes generated by the coils' electric currents [see Fig. 2(b)].

Fig. 2 shows a particular case where the z-coil is longitudinal to the applied flux and the x- and y-coils are transverse. To show separately the distribution of the primary and secondary fluxes, we assume in Fig. 2(a) zero currents in all the coils (this corresponds to a dc or very low-frequency case) and assume in Fig. 2(b) zero applied flux. To show in Fig. 2(b) the distribution of the secondary flux generated by the z-coil only, we assume zero currents in the x- and y-coils.

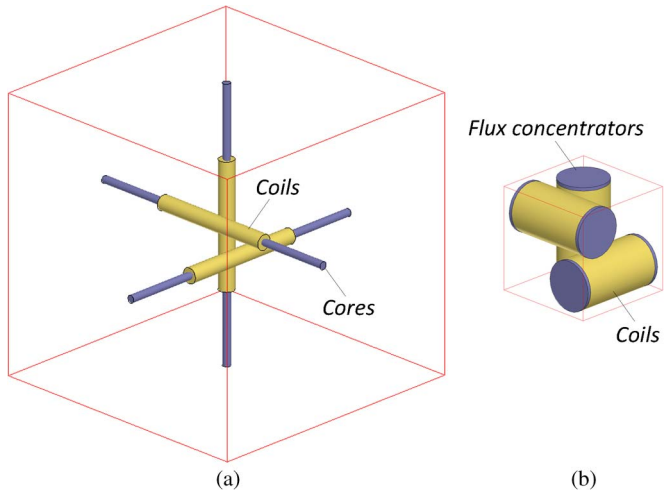

Fig. 1. Three-axial induction magnetometers with (a) low- and (b) high-density packing of the search coils.

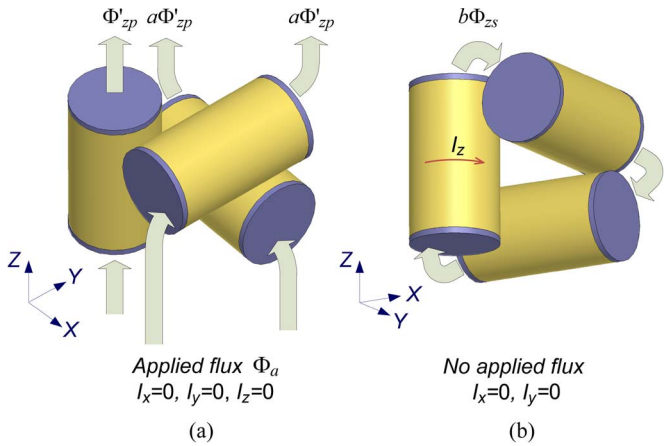

Fig. 2. Crosstalk due to (a) applied and (b) secondary fluxes. Note that the condition of zero currents in the coils in (a) is satisfied at dc and nearly satisfied at very low frequencies. To show in (b) the distribution of the secondary flux generated by the z-coil only, we assume zero currents in the x- and y-coils.

One can see from Fig. 2(a) that the applied flux, Φ_a, flows in not only the longitudinal coil, Φ'_{zp}, but also in the transverse coils, $a\Phi'_{zp}$, which provide an alternative path for it. Fig. 2(b) shows that the secondary flux, Φ_{zs}, of the z-coil is partially shunted, i.e., $b\Phi_{zs}$, by the transverse coils. As a result, not only the longitudinal coil but also the transverse coils are sensitive to the applied flux.

Manuscript received November 15, 2010; revised February 15, 2011; accepted February 18, 2011. Date of publication April 7, 2011; date of current version September 14, 2011. This work was supported in part by Analog Devices, Inc., by National Instruments, Inc., and by the Ivanier Center for Robotics Research and Production Management. The Associate Editor coordinating the review process for this paper was Dr. Salvatore Baglio.

The authors are with the Department of Electrical and Computer Engineering, Ben-Gurion University of the Negev, Beer-Sheva 84105, Israel.

Color versions of one or more of the figures in this paper are available online at http://ieeexplore.ieee.org.

Digital Object Identifier 10.1109/TIM.2011.2124850

The crosstalk strength depends on the packing density of the coils (see Fig. 1) and the frequency of the applied field. The crosstalk can be relatively weak (about 1%) at low frequencies [9], [10], where the first mechanism dominates, can be very strong [9] (above 50%) near resonance and moderate [9] (3%–6%) at high frequencies, where the second mechanism dominates.

In general, a crosstalk can be reduced by three different methods: 1) by reducing the strength of the crosstalk origin [1]–[10]; 2) by modifying the system configuration [8], [9], [11]–[15]; and 3) by measuring and excluding the crosstalk from the processed system output [16]–[20].

For example, the dominant crosstalk origins in three-axial induction magnetometers near their resonance are the electrical currents in the magnetometers' coils. Applying magnetic feedback [1]–[9] reduces these currents, thus reducing the strength of the crosstalk origin and, in this way, reducing the crosstalk. The same result can also be obtained by damping the resonance by connecting resistors in parallel to the magnetometers' coils [8], [10].

There are, however, principal limitations related to employing either magnetic feedback or damping resistors. The obtained reduction will still be limited at a level between the low- and high-frequency crosstalk values [9]. The coils' frequency response at resonance will be flattened [1]–[10]. This significantly reduces the magnetometer selectivity, which can be advantageous in many applications. Employing magnetic feedback also increases the magnetometer complexity and power consumption. An additional disadvantage of excessive dumping is that it significantly increases magnetometer noise.

An example of reducing crosstalk by modifying the system configuration is increasing the number of coils in three-axial magnetometers from three to six [9] or 12 [8] and arranging them symmetrically. Due to the symmetry, the total crosstalk in each channel is compensated. Examples of using symmetry or providing alternative paths for opposite crosstalk while modifying a system are given in [11]–[15] for inductive and capacitive types of coupling. A disadvantage of these methods is that they increase the system size and complexity.

Measuring and excluding the crosstalk from the system output can be obtained by employing additional hardware [16]. For example, the crosstalk between a number of inductive transmitters [16] operated at different frequencies can be reduced by measuring the crosstalk current components in each transmitter and then adding opposite excitation currents. However, such a method cannot be applied to the reduction of crosstalk in induction magnetometers, because their crosstalk is at the same frequency with the main signals.

Crosstalk can also be measured and excluded by employing special algorithms [17]–[20], without using any additional hardware. It can be done by considering the crosstalk components as unknowns in the measuring model and then finding and excluding them algorithmically. Such a "model-based" crosstalk compensation approach is used in this paper.

The aim of this paper is to reduce the crosstalk in three-axial inductive magnetometers while avoiding magnetic feedback. Instead, we reduce the crosstalk by using no additional hardware and only by processing the outputs of the magnetometer channels. Such compensation, aside from affecting the magnetometer selectivity, has an additional principal advantage: it allows, at least in theory, complete zeroing of the crosstalk. Naturally, inevitable systematic errors will limit the crosstalk compensation. Nevertheless, we show that, even in a practical case, the suggested compensation reduces the crosstalk much more efficiently than magnetic feedback.

II. Method

The total primary fluxes in the magnetometer coils can be given as follows:

$$\begin{cases} \Phi_{xp} = \Phi'_{xp} + a\left(\Phi'_{yp} + \Phi'_{zp}\right) + b(\Phi_{ys} + \Phi_{zs}) \\ \Phi_{yp} = \Phi'_{yp} + a\left(\Phi'_{xp} + \Phi'_{zp}\right) + b(\Phi_{xs} + \Phi_{zs}), \\ \Phi_{zp} = \Phi'_{zp} + a\left(\Phi'_{xp} + \Phi'_{yp}\right) + b(\Phi_{xs} + \Phi_{ys}) \end{cases} \quad (1)$$

where Φ'_{xp}, Φ'_{yp}, and Φ'_{zp} are the applied (crosstalk-free) primary fluxes; Φ_{xs}, Φ_{ys}, and Φ_{zs} are the total secondary fluxes; a is the ratio of the applied primary fluxes in the transverse and longitudinal coils, assuming that only the longitudinal coil is exposed to the applied flux and there are no electric currents in the coils [see Fig. 2(a)]; and b is the ratio of the secondary fluxes in the above coils, assuming that an excitation current is applied only to the longitudinal coil and there are no electric currents in the transverse coils [see Fig. 2(b)]. We assume for relatively small applied magnetic fields a linear behavior of the magnetization in the cores and flux concentrators and thus consider the a and b crosstalk factors as field independent.

To derive (1), we consider that, for example, the total primary flux Φ_{zp} in the z-core is combined from its crosstalk-free primary flux Φ'_{zp} [see Fig. 2(a)]; the fractions of the primary fluxes in the x- and y-cores Φ'_{xp} and Φ'_{yp}, respectively, leaking into the z-coil due to the first crosstalk mechanism in accordance to the a factor [see Fig. 2(a)]; and the fractions of the secondary fluxes in the x- and y-cores Φ_{xs} and Φ_{ys}, respectively, leaking into the z-coil due to the second crosstalk mechanism in accordance to the b factor [see Fig. 2(a)]. Φ_{xp} and Φ_{yp} are derived in a similar way.

Fig. 1(b) suggests that there should be some difference in the a factors for the x- and y-transverse coils. Our simulations, based on the finite-element method (FEM), show, however, that the a factors are nearly equal: the difference between them is less than 1%. Thus, we use, for the sake of simplicity, one and the same factor a in (1) for all the coils. According to the flux distribution in Fig. 2(b), there should be no difference in b factors.

The crosstalk-free primary fluxes in (1) can be related to the applied field components

$$\begin{cases} \Phi'_{xp} = B_{ax}\mu_{\text{app}}A \\ \Phi'_{yp} = B_{ay}\mu_{\text{app}}A, \\ \Phi'_{zp} = B_{az}\mu_{\text{app}}A \end{cases} \quad (2)$$

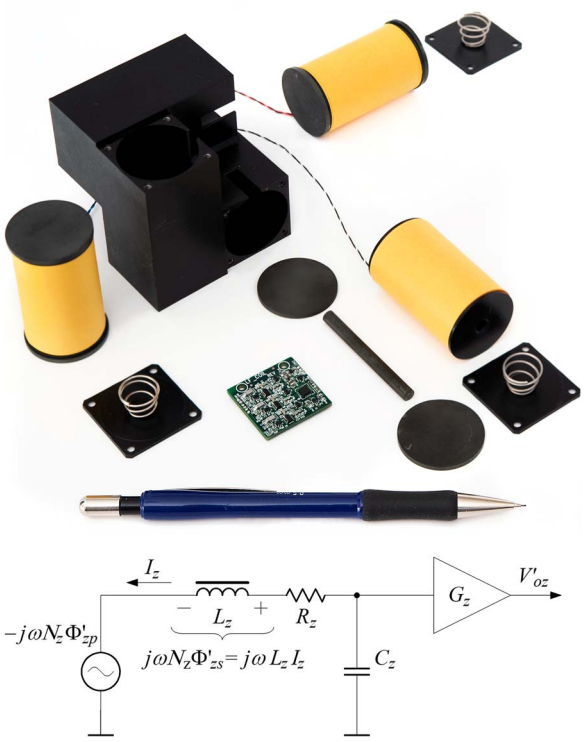

Fig. 3. Three-axial magnetometer (disassembled) and the equivalent electrical circuit of a single channel (with no crosstalk). The coils' parameters are given in Table I.

where μ_{app} is the core and flux concentrator apparent permeability, averaged over their cores' volumes, and A is the cross-sectional area of the cores.

Equation (1) can be rewritten in terms of the magnetometer outputs

$$\begin{cases} V_{ox} = V'_{ox} + a\left(\frac{V'_{oy}}{P_y} + \frac{V'_{oz}}{P_z}\right)P_x + b\left(\frac{V_{oy}}{S_y} + \frac{V_{oz}}{S_z}\right)P_x \\ V_{oy} = V'_{oy} + a\left(\frac{V'_{ox}}{P_x} + \frac{V'_{oz}}{P_z}\right)P_y + b\left(\frac{V_{ox}}{S_x} + \frac{V_{oz}}{S_z}\right)P_y, \\ V_{oz} = V'_{oz} + a\left(\frac{V'_{ox}}{P_x} + \frac{V'_{oy}}{P_y}\right)P_z + b\left(\frac{V_{ox}}{S_x} + \frac{V_{oy}}{S_y}\right)P_z \end{cases} \quad (3)$$

where V_{ox}, V_{oy}, and V_{oz} are the *total* magnetometer outputs; V'_{ox}, V'_{oy}, and V'_{oz} are the *crosstalk-free* magnetometer outputs; and (P_x, P_y, P_z) and (S_x, S_y, S_z) are the transfer functions between the coils' primary and secondary fluxes and the corresponding magnetometer outputs, respectively, such that, for a magnetometer coil, $\Phi_{zp} = V_{oz}/P_z$ and $\Phi_{zs} = V_{oz}/S_z$. (Note that, for a linear case, $\Phi'_{zp} = V'_{oz}/P_z$.) Equation (3) is obtained by substituting the fluxes in (1) with the corresponding voltages divided by the corresponding transfer functions.

For a magnetometer coil, Fig. 3 suggests that

$$P_z = \frac{V'_{oz}}{\Phi'_{zp}} = \frac{I_z\frac{1}{j\varpi C_z}G_z}{\Phi'_{zp}} = \frac{\frac{j\varpi N_z\Phi'_{zp}}{j\varpi L_z + R_z + \frac{1}{j\varpi C_z}}\frac{1}{j\varpi C_z}G_z}{\Phi'_{zp}} = \frac{j\varpi N_z G_z}{1 + j\varpi R_z C_z - C_z L_z \varpi^2}, \quad (4)$$

$$S_z = \frac{V'_{oz}}{\Phi'_{zs}} = I_z\frac{1}{j\varpi C_z}G_z\frac{N_z}{L_z I_z} = \frac{N_z G_z}{j\varpi C_z L_z}, \quad (5)$$

where N_z is the number of coil turns, L_z is the coil inductance, I_z is the coil current, G_z is the voltage gain of the preamplifier, ω is the angular frequency, and C_z is the coil capacitance.

The second and third terms in (3) represent the crosstalk components. Relative to the scalar crosstalk-free magnetometer output, the crosstalk components can be defined as follows:

$$\begin{cases} \delta v_x = \frac{|V_{ox} - V'_{ox}|}{\sqrt{V'^2_{ox} + V'^2_{oy} + V'^2_{oz}}} \\ \delta v_y = \frac{|V_{oy} - V'_{oy}|}{\sqrt{V'^2_{ox} + V'^2_{oy} + V'^2_{oz}}} \\ \delta v_z = \frac{|V_{oz} - V'_{oz}|}{\sqrt{V'^2_{ox} + V'^2_{oy} + V'^2_{oz}}}. \end{cases} \quad (6)$$

Equation (3) can be solved for the crosstalk-free magnetometer outputs

$$\begin{cases} V'_{ox} = \frac{1}{(a-1)(2a+1)}\left[(1+a+2abP_x/S_x)V_{ox} - \frac{a+bP_y/S_y}{P_y/P_x}V_{oy} - \frac{a+bP_z/S_z}{P_z/P_x}V_{oz}\right] \\ V'_{oy} = \frac{1}{(a-1)(2a+1)}\left[(1+a+2abP_y/S_y)V_{oy} - \frac{a+bP_x/S_x}{P_x/P_y}V_{ox} - \frac{a+bP_z/S_z}{P_z/P_y}V_{oz}\right] \\ V'_{oz} = \frac{1}{(a-1)(2a+1)}\left[(1+a+2abP_z/S_z t)V_{oz} - \frac{a+bP_x/S_x}{P_x/P_y}V_{ox} - \frac{a+bP_y/S_y}{P_y/P_x}V_{oy}\right]. \end{cases} \quad (7)$$

Thus, processing the magnetometer outputs in accordance with (7) allows the compensation of the crosstalk.

III. Experiment

To validate the suggested crosstalk compensation, we have built and tested a three-axial induction magnetometer. The parameters of its coils are given in Table I. The coils were positioned within a plastic housing (see Fig. 3) that was fabricated with high precision to obtain the best possible mechanical orthogonality. The magnetometer was placed into a three-shell magnetic shield to avoid electromagnetic interference. An external magnetic field was applied with a long solenoid along the z-coil axis; thus, the applied primary fluxes in the x- and y-channels in (1) and the corresponding magnetometer crosstalk-free outputs in (3) were equal to zero: $\Phi'_{xp} = 0$, $\Phi'_{yp} = 0$, and $V'_{xp} = 0$, $V'_{yp} = 0$.

To increase the signal-to-noise ratio of measurements (see Fig. 4), the magnitude of the excitation current in the solenoid was automatically adjusted to keep the z-channel output near its maximum. The excitation current magnitude and the

TABLE I
PARAMETERS OF THE MAGNETOMETER CHANNELS

Coil parts	Parameters		
Flux concentrators	30 mm diameter, 2 mm thickness		
Core	5 mm diameter, 50 mm length		
Relative magnetic permeability of the core and flux concentrators	2000		
Copper wire	35-μm diameter (39-μm with isolation)		
Winding	330 thousands of turns, 6 mm inner diameter, 29 mm outer diameter, 47 mm length		
The shortest distances between the coils' axes	32 mm		
Coils	x	y	z
dc resistance (kΩ)	309.133	269.335	304.951
inductance (kH)	8.411	8.866	8.768
tuning capacitance (nT)	4.7	5.45	5.49
Crosstalk coefficients (%)	a		b
	0.91		5.24
Preamplifier gain	1000		

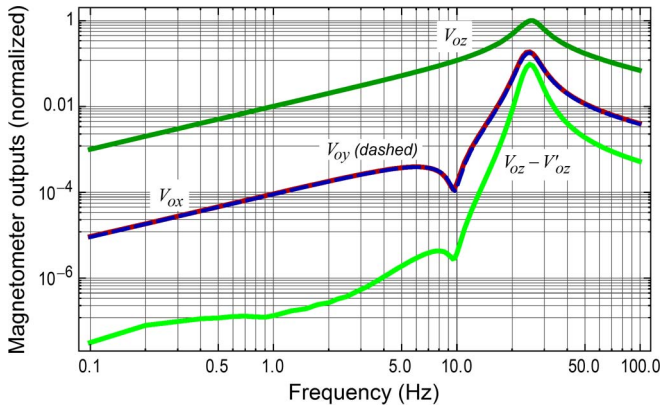

Fig. 4. Magnetometer frequency response.

magnetometer outputs (see Fig. 4) were processed with a National Instruments data acquisition system.

The frequency responses of the magnetometer channels are shown in Fig. 4. Since there are no applied fields in the x- and y-directions, the x- and y-channel outputs represent, according to (3), the corresponding crosstalk components.

Relative to V'_{oz}, the crosstalk components without compensation are found in Fig. 5 as

$$\begin{cases} \delta v_x = \left| \frac{V_{ox}}{V'_{oz}} \right| \\ \delta v_y = \left| \frac{V_{oy}}{V'_{oz}} \right| \\ \delta v_z = \left| \frac{V_{oz} - V'_{oz}}{V'_{oz}} \right|. \end{cases} \tag{8}$$

The a factor in (3) was found as the crosstalk value measured at low frequencies (see Fig. 5) in channels x and y. This is because, at low frequencies, the crosstalk due to the secondary fluxes can be neglected, and, according to (3) and (6) for $V'_{xp} = 0$ and $V'_{yp} = 0$, the crosstalk becomes $\delta v_x = aV'_{oz}P_x/(V'_{oz}P_z)$ and $\delta v_y = aV'_{oz}P_y/(V'_{oz}P_z)$. For $P_x \approx P_z$ and $P_y \approx P_z$, $\delta v_x \approx a$, and $\delta v_y \approx a$.

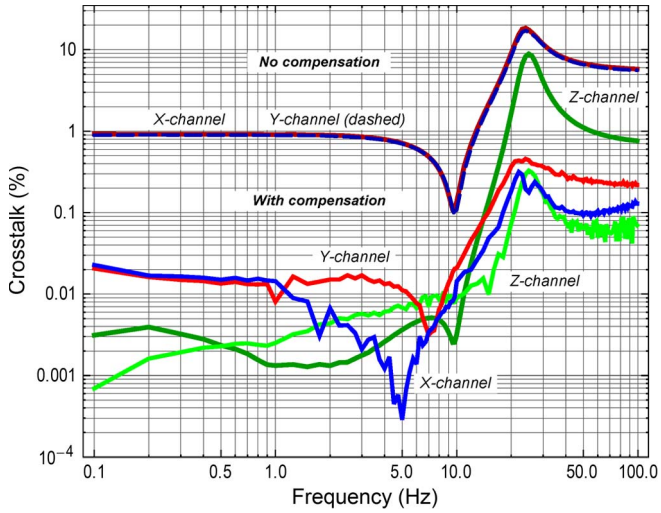

Fig. 5. Compensation of the magnetometer crosstalk.

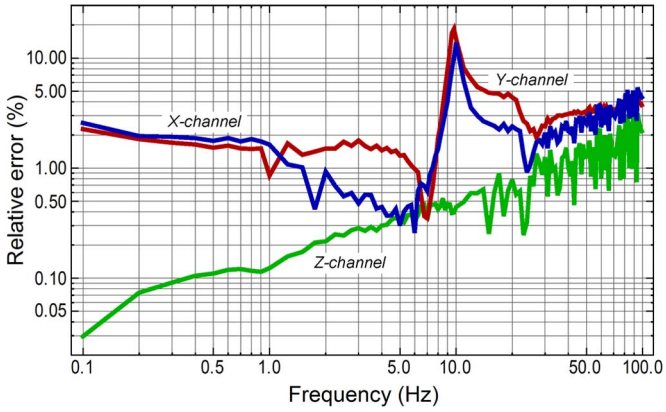

Fig. 6. Relative errors between the measured (V_{ox}, V_{oy}, and V_{oz}) and estimated ($\hat{V}_{ox}$, $\hat{V}_{oy}$, and $\hat{V}_{oz}$) magnetometer frequency responses.

The coil electric parameters (resistance, inductance, and capacitance), the crosstalk coefficient b (see Table I), and V'_{oz} were set at those values that provide the best fitting (see Figs. 6 and 7) between the measured (V_{ox}, V_{oy}, and V_{oz}) and estimated (3) ($\hat{V}_{ox}$, $\hat{V}_{oy}$, and $\hat{V}_{oz}$) magnetometer outputs. The obtained values were used in (7) to process the measured magnetometer outputs and compensate the crosstalk. Since the *estimated* values of the coil electric parameters, the a and b factors, and V'_{oz} were used in (7), instead of the *true* values, we denote the solutions of (7) as $\hat{V}'_{ox}$, $\hat{V}'_{oz}$, and $\hat{V}'_{oz}$.

Relative to V'_{oz}, the crosstalk components with compensation are found in Fig. 5 as

$$\begin{cases} \delta \hat{v}_x = \left| \frac{\hat{V}'_{ox}}{V'_{oz}} \right| \\ \delta \hat{v}_y = \left| \frac{\hat{V}'_{oy}}{V'_{oz}} \right| \\ \delta \hat{v}_z = \left| \frac{\hat{V}'_{oz}}{V'_{oz}} \right|. \end{cases} \tag{9}$$

Fig. 5 shows that, without compensation, the x- and y-crosstalk components vary from 0.91% at low frequencies to 20% near resonance and to 5.7% at high frequencies. The longitudinal z-crosstalk component is notable only near resonance,

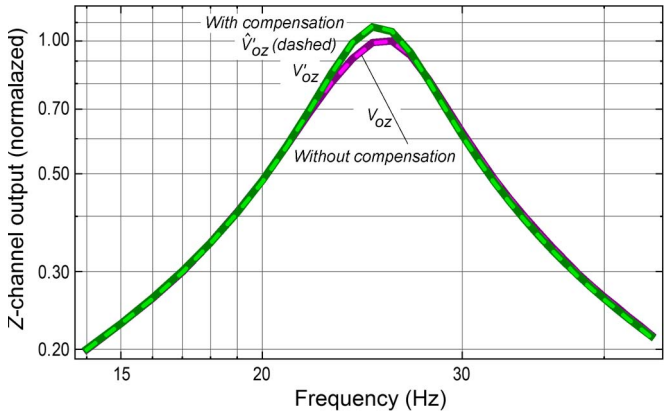

Fig. 7. Output voltage of the longitudinal z-channel. The solid bottom curve is the measured output V_{oz}. The coinciding dashed curve is the fitted output $\hat{V}_{oz}$. The solid top curve is the theoretical output with no crosstalk V'_{oz}. The coinciding dashed curve is the compensated output $\hat{V}'_{oz}$.

where it approaches 10%. At low frequencies, this component rapidly decreases down to the measurements' noise floor.

Fig. 5 also shows that the compensation reduces crosstalk below 0.5% in the whole frequency range. At low frequencies, the compensation is even better: the crosstalk is reduced down to about 0.02%.

To compare the suggested crosstalk compensation method against the crosstalk reduction by applying magnetic feedback, we considered the equivalent electrical circuit given in Fig. 8, where M_z is the mutual inductance between the magnetometer and feedback coils, I_{fz} is the feedback coil current, and R_{fz} is the feedback resistor value. For this electrical circuit, the primary and secondary transfer functions can be given as follows, assuming that the R_{fz} value is much higher than the other part of the impedance at the feedback coil terminals, i.e.,

$$P_{zf} = \frac{V'_{oz}}{\Phi'_{zp}} = \frac{V'_{oz}}{\frac{j\varpi(L_z I_z + M_z I_{zf}) + I_z\left(R_z + \frac{1}{j\varpi C_z}\right)}{j\varpi N_z}}$$
$$= \frac{j\varpi N_z V'_{oz}}{j\varpi\left(L_z \frac{V'_{oz}/G_z}{\frac{1}{j\varpi C_z}} + M_z \frac{V'_{oz}}{R_{fz}}\right) + \frac{V'_{oz}/G_z}{\frac{1}{j\varpi C_z}}\left(R_z + \frac{1}{j\varpi C_z}\right)}$$
$$= \frac{j\varpi N_z G_z}{1 + j\varpi\left(R_z C_z + \frac{M_z G_z}{R_{fz}}\right) - C_z L_z \varpi^2} \quad (10)$$

$$S_{zf} = \frac{V'_{oz}}{\Phi'_{zp}} = \frac{V'_{oz}}{\frac{L_z I_z + M_z I_{zf}}{N_z}} = \frac{V'_{oz}}{\frac{L_z I_z + M_z \frac{V'_{oz}}{R_{fz}}}{N_z}}$$
$$= \frac{I_z \frac{1}{j\varpi C_z} G_z}{\frac{L_z I_z + M_z \frac{I_z \frac{1}{j\varpi C_z} G_z}{R_{fz}}}{N_z}} = \frac{N_z}{j\varpi C_z \frac{L_z}{G_z} + \frac{M_z}{R_{fz}}}. \quad (11)$$

Considering (3), (6), (10) and (11), we have calculated the theoretical crosstalk with magnetic feedback (see Fig. 9) for $M_z = k_z (L_z L_{fz})^{0.5}$, the coupling coefficient $k = 1$, $L_f = 0.1$ mH, and $R_f = 70$ kΩ. (It is assumed that all the coils have similar k, L_f, and R_f parameters.)

Fig. 9 shows that magnetic feedback is unable to reduce the x and y crosstalk components below 0.91% at low frequencies and below 5.7% at high frequencies. The longitudinal z-crosstalk component is also reduced less efficiently than by the compensation method. Fig. 10 shows that applying magnetic feedback significantly reduces the coil selectivity.

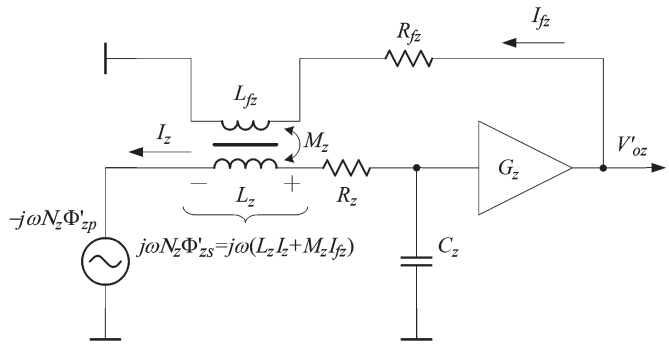

Fig. 8. Equivalent electrical circuit of a magnetometer channel with magnetic feedback (with no crosstalk).

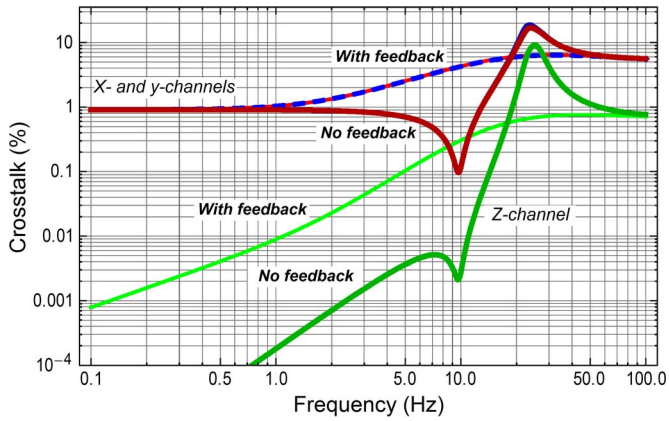

Fig. 9. Reduction of the magnetometer crosstalk with magnetic feedback.

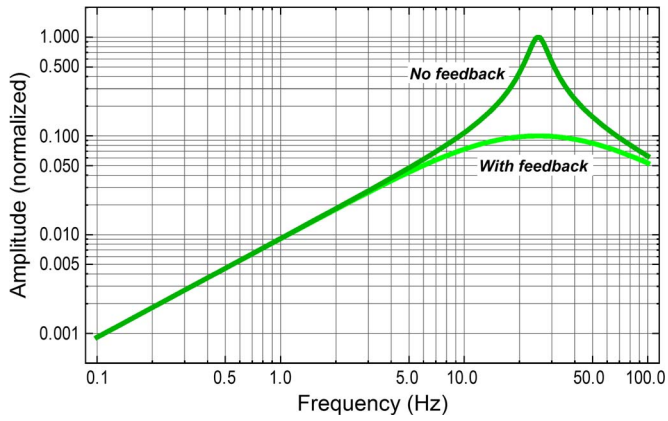

Fig. 10. Theoretical frequency responses of the magnetometer longitudinal channel (bright curve) with and (dark curve) without feedback.

IV. Conclusion

It has been shown that crosstalk in three-axial induction magnetometers can be significantly reduced without employing additional hardware, only by processing the magnetometer outputs. The compensation algorithm (7) is based on the approximate magnetometer model (see Fig. 3), where the coils are described by linear lumped electric coil parameters: resistance, inductance, and capacitance.

The crosstalk caused by the applied flux is described by a factors, and the crosstalk caused by the secondary fluxes is described by b factors. The difference in a factors for different coils have been found below 1% with the help of FEM simulations, and these factors are assumed to be equal for all the coils. There should be no difference in b factors for different coils, because the secondary flux of each coil is shunted by the other coils in a similar way.

The a factor was estimated as the crosstalk value measured at low frequencies in channels x and y. To estimate the electric coil parameters, the b crosstalk factor, and the applied field, best matching between the measured and modeled magnetometer frequency responses was found. The matching errors (see Fig. 6) are 10%–20% at 10 Hz, 1%–2% at lower frequencies, and below 5% at higher frequencies.

The inevitable systematic errors related to the magnetometer model approximation and the estimation of the model parameters limit the crosstalk compensation. It is shown, however, that the compensation is nevertheless very efficient (see Fig. 5). For the x- and y-coils, the crosstalk has been reduced by a factor of 30–50: from about 1% down to 0.02% at low frequencies, from 20% down to 0.5% at resonance, and from 6% down to 0.2% at high frequencies. For the z-coil, the crosstalk has been reduced by a factor of 30 at resonance (from about 9% down to 0.3%) and by a factor of 10 at high frequencies (from 0.7% down to 0.07%). At dc and low frequencies, the crosstalk in the z-coil is practically absent (below 0.01%) since the fluxes applied to the x- and y-coil are equal to zero, i.e., $\Phi'_{xp} = 0$ and $\Phi'_{yp} = 0$, and the secondary fluxes, Φ_{xs} and Φ_{xs}, are very low (equal to zero at dc). The compensation is unable to reduce such a very low crosstalk. It actually increases a bit, but the resultant crosstalk is still below 0.01%.

For comparison, employing magnetic feedback is much less efficient (see Fig. 9). For the x- and y-coils, the crosstalk at resonance is reduced by a factor less than 4: from about 20% down to 6%. There is no crosstalk reduction at both low and high frequencies. At frequencies just below resonance, the crosstalk is significantly increased. For the z-coil, the crosstalk at resonance is reduced by a factor of 13 (from about 9% down to 0.7%). At frequencies just below resonance, this crosstalk is significantly increased.

In contrast to magnetic feedback, the suggested compensation does not also affect the magnetometer selectivity.

The crosstalk compensation efficiency may still be increased by more accurate modeling of the magnetometer; however, from a practical point of view, the reached maximum crosstalk of 0.5% well suits even most demanding applications. Such a low crosstalk results in the maximum uncertainties in the measured field direction and magnitude of about 0.4° and 1%, respectively.

REFERENCES

[1] C. Coillot, J. Moutoussamy, P. Leroy, G. Chanteur, and A. Roux, "Improvements on the design of search coil magnetometer for space experiments," *Sensor Lett.*, vol. 5, no. 1, pp. 167–170, Mar. 2007.

[2] E. Paperno and A. Grosz, "A miniature and ultralow power search coil optimized for a 20 mHz to 2 kHz frequency range," *J. Appl. Phys.*, vol. 105, no. 7, p. 07E 708, Apr. 2009.

[3] A. Grosz, E. Paperno, S. Amrusi, and E. Liverts, "Integration of the electronics and batteries inside the hollow core of a search coil," *J. Appl. Phys.*, vol. 107, no. 9, p. 09E 703, May 2010.

[4] R. Sklyar, "Induction field transducers stability limits," *IEEE Sensors J.*, vol. 5, no. 5, pp. 924–928, Oct. 2005.

[5] H. C. Séran and P. Fergeau, "An optimized low-frequency three-axis search coil magnetometer for space research," *Rev. Sci. Instrum.*, vol. 76, no. 4, p. 044 502, Apr. 2005.

[6] J. B. Cao, Z. X. Liu, J. Y. Yang, C. X. Yian, Z. G. Wang, X. H. Zhang, S. R. Wang, S. W. Chen, W. Bian, W. Dong, Z. G. Zhang, F. L. Hua, L. Zhou, N. Cornilleau-Wehrlin, B. de Laporte, M. Parrot, H. Alleyne, K. Yearby, O. Santolıacute;k, and C. Mazelle, "First results of low frequency electromagnetic wave detector of TC-2/Double Star program," *Annales Geophysicae*, vol. 23, no. 8, pp. 2803–2811, 2005.

[7] A. Roux, O. Le Contel, C. Coillot, A. Bouabdellah, B. de la Porte, D. Alison, S. Ruocco, and M. C. Vassal, "The search coil magnetometer for THEMIS," *Space Sci. Rev.*, vol. 141, no. 1–4, pp. 265–275, Dec. 2008.

[8] J. C. Dupuis, "Optimization of a 3-axis induction magnetometer for airborne geophysical exploration," M.Sc. thesis, Univ. New Brunswick, Fredericton, NB, Canada, 2001.

[9] A. Grosz, E. Paperno, S. Amrusi, and T. Szpruch, "Minimizing crosstalk in three-axial induction magnetometers," *Rev. Sci. Instrum.*, vol. 81, no. 12, p. 125 106, Dec. 2010.

[10] T. Tosaka, I. Nagano, and S. Yagitani, "Development of a magnetic field measurement system using a tri-axial search coil," in *Proc. IEEE EMC Symp.*, Chicago, IL, Aug. 2005, pp. 102–106.

[11] T. T. Yan and M. Z. Jenu, "Capacitive and inductive couplings of PCB traces," in *Proc. IEEE Region 10 Int. Conf., TENCON*, Kuala Lumpur, Malaysia, Sep. 24–27, 2000, pp. 186–191.

[12] M. Samplón, J. S. Artal, J. Letosa, A. Usón, and F. J. Arcega, "Evaluation of errors associated with crosstalk magnetic fields using finite element method in high electrical current measurement," in *Proc. ICREPQ*, Zaragoza, Spain, Mar. 16–18, 2005.

[13] J. J. Abbot and R. K. Kunze, "Micro-strip crosstalk compensation using stubs," U.S. Patent Application Publication, 2010/0327989 A1, Dec. 30, 2010.

[14] A. H. McCurdy, J. R. Pharney, D. L. Reed, T. E. Steele, and P. H. Straub, "Inductive crosstalk compensation in a communication connector," U.S. Patent 6 443 777, Sep. 3, 2002.

[15] T. H. Conorich, M. G. German, and A. I. Hashim, "Electrical connector with crosstalk compensation," U.S. Patent 5 716 237, Feb. 10, 1998.

[16] N. Tziony, M. Itzkovich, and N. Moriya, "Electrical circuit for crosstalk reduction," U.S. Patent 6 711 215, Mar. 23, 2004.

[17] A. Plotkin, O. Shafrir, E. Paperno, and D. M. Kaplan, "Magnetic eye tracking: A new approach employing a planar transmitter," *IEEE Trans. Biomed. Eng.*, vol. 57, no. 5, pp. 1209–1215, May 2010.

[18] M. Steinlin, S. Weikert, and K. Wegener, "Open loop inertial cross-talk compensation based on measurement data," in *Proc. 25th Annu. Meeting Amer. Soc. Precision Eng.*, Atlanta, GA, Oct. 31–Nov. 4, 2010.

[19] C. D. Onal, B. Sümer, and M. Sitti, "Cross-talk compensation in atomic force microscopy," *Rev. Sci. Instrum.*, vol. 79, no. 10, pp. 103 706-1–103 706-7, Oct. 2008.

[20] D. Schrand, Crosstalk Compensation Using Matrix Methods. [Online]. Available: http://www.eetindia.co.in/STATIC/PDF/200808/EEIOL_2008AUG13_SIG_TA_01.pdf?SOURCES=DOWNLOAD

Eugene Paperno received the B.Sc. and M.Sc. degrees in electrical engineering from the Minsk Institute of Radio Engineering, Minsk, Republic of Belarus, in 1983 and the Ph.D. degree (*summa cum laude*) from the Ben-Gurion University of the Negev, Beer-Sheva, Israel, in 1997.

From 1983 to 1991, he was with the Institute of Electronics, Belorussian Academy of Sciences, Minsk. From 1997 to 1999, he was a Japan Society for the Promotion of Science Postdoctoral Fellow with Kyushu University, Fukoka, Japan. Since 1999, he has been with the Department of Electrical and Computer Engineering, Ben-Gurion University of the Negev. His current research interests include magnetic sensors, atomic magnetometers, magnetic shielding, magnetic tracking, and magnetic and electronic instrumentation.

Asaf Grosz received the B.Sc. degree in physics and computer science from Tel Aviv University, Tel Aviv, Israel, in 2007. He is currently working toward the M.Sc. degree at the Department of Electrical and Computer Engineering, Ben-Gurion University of the Negev, Beer-Sheva, Israel. His current research interests include magnetometry, magnetic sensors, and low-noise ultralow-power electronics.

Shai Amrusi received the B.Sc. degree in electrical and computer engineering from the Ben-Gurion University of the Negev, Beer-Sheva, Israel, in 2007, where he is currently working toward the M.Sc. degree at the Department of Electric and Computer Engineering.

His current research interests are magnetic tracking systems and magnetic sensors.

Boris Zadov received the B.Sc. degree in electrical and computer engineering from the Sami Shamoon College of Engineering, Beer-Sheva, Israel, in 2007. He is currently working toward the M.Sc. degree at the Department of Electrical and Computer Engineering, Ben-Gurion University of the Negev, Beer-Sheva.

His current research interests include magnetometry, magnetic sensors, and low-noise ultralow-power electronics.